Radiation Effects & Defects in Solids, Vol. 149, pp. 279–286

TSDC PROBE OF ANISOTROPIC POLARIZABILITY IN FLUORAPATITE SINGLE CRYSTALS

A. VASSILIKOU-DOVA[a,*], B. MACALIK[b], I.M. KALOGERAS[a], M. CALAMIOTOU[a], C.A. LONDOS[a] and L. FYTROS[a]

[a]*Solid State Physics Section, Physics Department, University of Athens, Panepistimiopolis, 157 84 Zografos, Greece;* [b]*Institute of Low Temperature and Structure Research, Polish Academy of Sciences, 50-950 Wroclaw, Poland*

(Received 6 July 1998; In final form 20 September 1998)

A study of single phase hexagonal fluorapatite crystals from Durango (Mexico), by means of the TSDC technique, has demonstrated a variety of dielectric relaxation mechanisms for different poling orientations, parallel and perpendicular to the crystallographic *c*-axis. In the first case, the TSDC spectrum consists of a broad complex current band, featuring a distribution of the pertinent energy barriers. In the case of perpendicular electric stimulus ($E_p \perp c$) the overall intensity of the relaxation spectrum is reduced by at least one order of magnitude, compared to that with $E_p \parallel c$ axis, with at least five highly overlapping dielectric bands. A tentative attribution of the anisotropic polarizability observed in the two different orientations to specific micromolecular mechanisms takes into account the creation and selective partitioning of several microstructural defects (e.g. limited Cl^- and REE^{3+} substitution for F^- and Ca^{2+} respectively, ionic vacancies and dislocations). These types of defects produce several kinds of (re)orientable dipolar units and permit short range motions of electric charges, which are both directly detectable by dielectric relaxation spectroscopy methods.

Keywords: Fluorapatites; Dielectric relaxation; Thermally stimulated depolarization currents

* Corresponding author. E-mail: avasilik@cc.uoa.gr.

1. INTRODUCTION

Apatites, $Ca_{10}(PO_4)_6(F, OH, Cl)_2$, constitute a group of minerals that comprises members of high technological exploitation [1]. The fluorapatitic structure consists of PO_4 tetrahedra arranged in trees around hexad axes, forming tubes parallel to *c*-axis with fluorine ions along their axis. Six out of the 10 calcium ions in the apatitic unit cell, occupy the so-called Ca(2) site (Fig. 1). These ions line the tubes internally and tie in the F anions. Each of Ca(2) ions (co-ordination number VII) is one of the triad that surrounds a F^- ion at each corner of the unit cell. The remaining Ca^{2+} ions lying between the tubes simply link neighboring tubes, and occupy the so-called Ca(1) sites (co-ordination number IX). The complicated apatitic framework and the multiplicity of atomic substitutions offer a prominent background for the creation of ion vacancies, electrical dipoles or extended dipolar complexes, whose dielectric response is expected to be anisotropic. Insofar, the TSDC

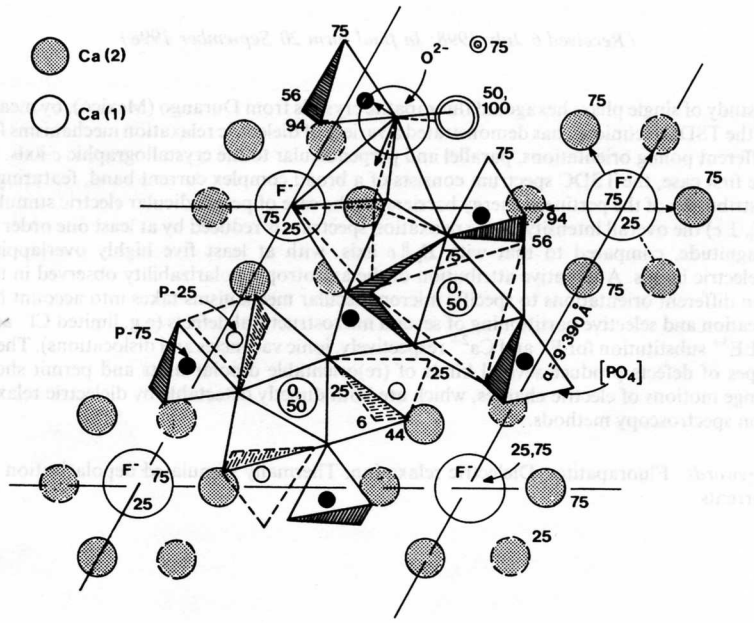

FIGURE 1 Polyhedral model of the fluorapatitic structure projected on the (0001) plane. Elevations are represented as percentages of *c*. Mirror planes are located at 0.25 and 0.75 *c*.

technique has been successfully applied in studies of various apatites in compressed polycrystalline form, although experiments in monocrystals give evidence for the existence of anisotropy in dielectric polarizability along different crystallographic orientations. In the present paper we report results on several temperature dependent dipolar or dipolar-like ionic motions that contribute to a change in the dielectric polarizability of fluorapatite along preferred polarization orientations.

2. EXPERIMENTAL

Samples of transparent, light yellow-greenish, fluorapatite of gem quality from Cerro de Mercado (Durango, Mexico), virtually free from inclusions and mineral coatings, were cut from a large prismatic crystal (approx. $3\frac{1}{4}$cm long by $1\frac{1}{2}$cm wide) parallel and perpendicular to the crystallographic c-axis, using the natural faces as a guide. The X-ray diffraction pattern ($2\theta = 20-90°$) was recorded employing a Siemens D5000 powder diffractometer with CuKα radiation and a secondary monochromator at RT. The corresponding Rietveld analysis (factor $R_{wp} = 11.13$, [2]) has showed single phase hexagonal fluorapatite, $a = 9.3921(2)$ Å, $c = 6.8830(2)$ Å, with a space group $P6_3/m$. The X-ray fluorescence (XRF) trace-element analysis, presented in Table I, reveals the presence of an appreciable amount of rare earth elements (REE). Several other light substitute ions (like, Mn^{2+}, Si^{4+}, Na^+, K^+ and Cl^-),

TABLE I Trace-element analysis of fluorapatite crystals (Cerro de Mercado, Durango, Mexico) obtained by X-ray fluorescence

Substitution for	*Trace ion*	*Analysis* (ppm)
P^{5+}	As^{5+}	2668 ± 90
Ca^{2+}	Sr^{2+}	497 ± 15
	Y^{3+}	823 ± 24
	La^{3+}	2398 ± 218
	Ce^{3+}	2736 ± 288
	Pr^{3+}	319 ± 32
	Nd^{3+}	990 ± 100
	Sm^{3+}	134 ± 13
	Gd^{3+}	99 ± 10
	Th^{3+}	418 ± 21
	U^{3+}	15.3 ± 1.5

are also expected to enrich fluorapatite. The TSDC experimental setup has been discussed in a previous publication [2].

3. RESULTS AND DISCUSSION

The thermally stimulated currents spectrum recorded for the $E_p \parallel c$ poling condition is depicted in Fig. 2 (plot a). The spectrum is dominated by an extended current signal (HT band) maximizing around 300 K, which covers the entire temperature range under investigation.

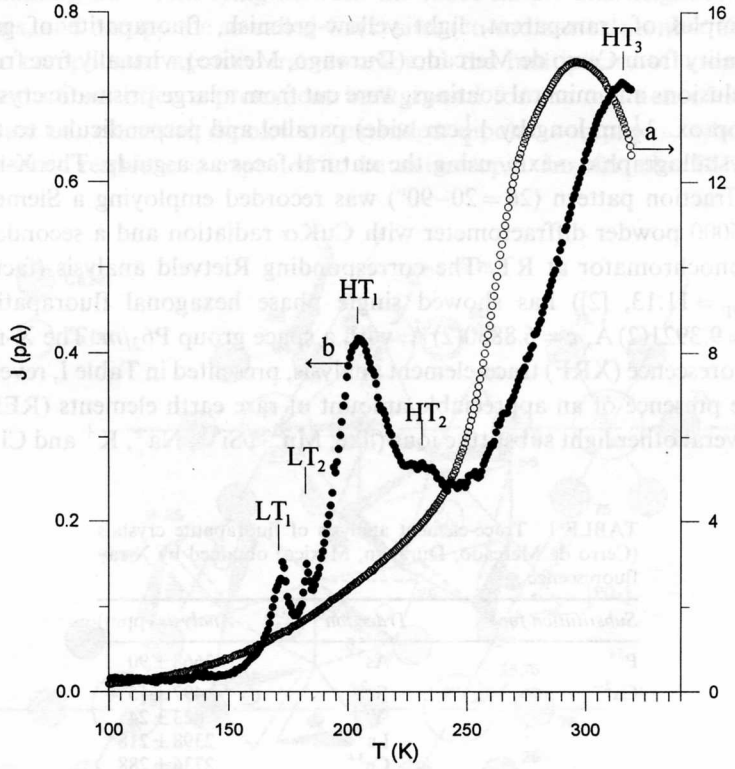

FIGURE 2 TSDC spectra for fluorapatite polarized with (a) the electric field parallel to c-axis ($E_p \parallel c$-axis), and (b) perpendicular to c-axis ($E_p \perp c$-axis). The thermostimulated current discharge curves were measured with the testing materials under vacuum ($\cong 10^{-4}$–10^{-5} Torr), in stainless steel electrodes electrolytically covered by chromium. The experimental conditions were: $T_p = 320$ K, $E_p = 18$ kV/cm, $t_p = 5$ min, and cooling/heating rates of 5.0 ± 0.2 degrees/min.

In order to decompose the band and obtain the activation energy spectrum of the relaxation mechanisms involved, we applied the partial discharge method in the temperature range of 110–320 K, calculating activation energy parameters between 0.15 and 0.85 eV. Although there is no clear evidence for some stepwise changes in the plot of activation energy E vs. the middle-point of the discharge temperature range of each cycle T_{mp} (Fig. 3), within the experimental errors, there appears to be an accumulation of the energy barriers in the temperature range 210 ± 20 K around 0.53 ± 0.03 eV.

The thermogram of a sample with E_p perpendicular to the crystallographic c-axis (Fig. 2, plot b) demonstrates five overlapping bands that peak at approximately 172 K (denoted as LT_1 band), 183 K (LT_2), 206 K (HT_1), 235 K (HT_2), and 316 K (HT_3). Variations in the electric field, polarization temperatures T_p and times t_p are supportive of a dipolar interpretation for the three low temperature bands (LT_1, LT_2

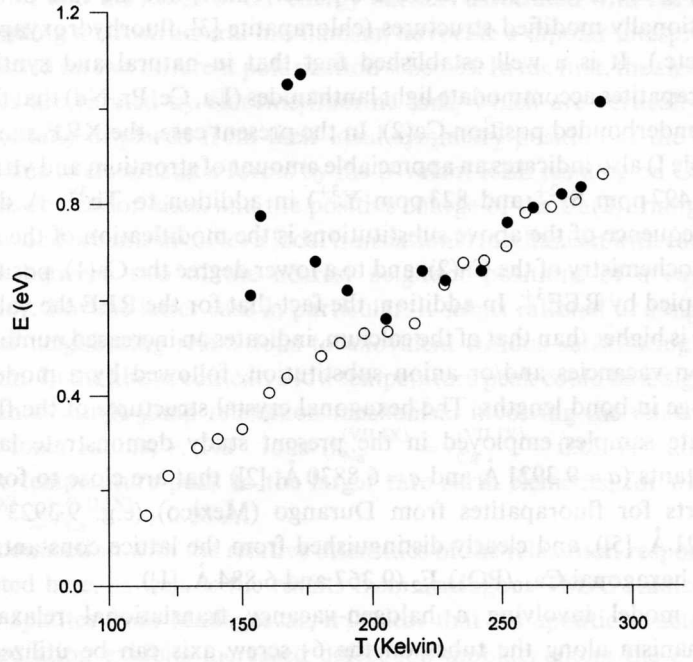

FIGURE 3 Plot of the activation energies E vs. the middle-point temperature of the partial TSDC discharge cycles T_{mp} for (a) $E_p \parallel c$-axis (○), and (b) $E_p \perp c$-axis (●).

and HT_1). The straight line fitting of the Arrhenius plot for the lower part of the thermostimulated currents spectrum, which coincides with the rising left wing of LT_1 peak, results to a (re)orientation activation energy of $E_1 = 0.38 \pm 0.02$ eV. In the temperature range of the weak but highly reproducible LT_2 signal we observe a sudden sharp increase in the energy values with a maximum at $E_2 = 0.86 \pm 0.03$ eV. The activation energy spectrum in the region of the HT_1 and HT_2 bands, around 200–240 K, varies between $E_3 = 0.60$–0.70 eV. The strong HT_3 band (plot b, Fig. 2) is characterized by an energy barrier, E_4, around 0.82 eV.

The preconditions for the development of macroscopic dielectric polarizability and charge storage at low temperatures are fulfilled if one takes into account in detail the apatite's crystal structure data. In fluorapatite, the 6_3 axis of F^- ions (at $z = 1/4, 3/4c$ in the hexagonal cell) passes perpendicularly to the planes of the adjacent Ca(2) triangles and through their centers. In the pure stoichiometric form of the fluorapatite crystals, the F^- ion occupies exactly the center of the Ca triangle, precluding the formation of electric dipoles. This is not the case of compositionally modified structures (chlorapatite [3], fluorhydroxyapatite [4], etc.). It is a well established fact that in natural and synthetic fluorapatites accommodate light lanthanides (La, Ce, Pr, Nd) that favor the underbonded position Ca(2). In the present case, the XRF analysis (Table I) also indicates an appreciable amount of strontium and yttrium (i.e. 497 ppm Sr^{2+} and 823 ppm Y^{3+}) in addition to Th^{3+}. A direct consequence of the above substitutions is the modification of the total stereochemistry of the Ca(2), and to a lower degree the Ca(1), positions occupied by REE^{3+}. In addition, the fact that for the REE the valence state is higher than that of the calcium, indicates an increased number of cation vacancies and/or anion substitution, followed by a moderate change in bond lengths. The hexagonal crystal structures of the fluorapatite samples employed in the present study demonstrate lattice constants ($a = 9.3921$ Å and $c = 6.8830$ Å, [2]) that are close to former reports for fluorapatites from Durango (Mexico) (e.g. 9.3923 and 6.8821 Å, [5]), and clearly distinguished from the lattice constants for pure hexagonal $Ca_{10}(PO_4)_6F_2$ (9.367 and 6.884 Å, [1]).

A model involving a halogen-vacancy translational relaxation mechanism along the tubes on the 6_3 screw axis can be utilized to describe the presence of the strong thermocurrent signals appearing in the TSDC spectra recorded for fluorapatite in the $E_p \parallel c$ poling

condition. The existence of an increasing trend of the (re)orientational activation energies with scanning temperature can be therefore connected with the presence of a distribution of microdomains in space along the *c*-axis with different local environment for the vacancies. The above mechanism is most likely joined by contributions of other strongly overlapping relaxations. The enhanced ionic mobility in this case can also be connected with the presence of pure screw dislocations that align with the crystallographic *c*-axis, and mixed dislocations with a slight deviation from alignment with the *c*-axis [6]. The corresponding distortion in the inter-ionic distances provide easy paths for short range migration of ions, especially by virtue of their relative aligning with the poling axis.

In relation to the $E_p \perp c$ experiments, the assignment of individual bands to definite mechanisms in microstructural level is connected with the creation and spatial distribution of certain structural defects [2]. As regards the LT relaxation domains, both their dipolar-type compatible behavior and the range of the energy barriers associated with the corresponding microstructural mechanism, advocate a dipolar interpretation based on two different polarization schemes. In the first, the electric dipoles are formed by chlorine/fluorine ions, which are vertically or horizontally displaced from their ideal symmetry position at the columns due to electrostatic forces by the trivalent REE residing on Ca(2) and nearby cation sites, and the positive charge of the Ca(2)-triangles. The second scheme involves a local translational mechanism with cation jumps between two of the nearest neighbor positions of a cation vacancy. For the latter case in particular, it seems rational to assign a pair of neighboring relaxations to aliovalent cations substituting for calcium. In the above context, a low temperature peak could be assigned to a short range jump relaxation mechanism involving the relatively small ionic radius, r, Na^+ ions ($r_{Na}^{(VII,IX)} = r_{Ca}^{(VII,IX)} - 0.02$ Å), and a higher temperature peak to the larger rare earth elements, for which $r_{REE}^{(VII,IX)} \geq r_{Ca}^{(VII,IX)} + 0.05$ Å.

In connection with the relative intensities of the relaxation responses reported here, as well as the results from analogous TSDC studies of green apatites from Madagascar, it is clear that the apatitic structural configuration exhibits increased defect ion mobility along the *c*-axis direction. This observation is essential for the practical electrical and biomedical applications of the synthetic products and stresses the

importance and necessity for single crystal experimental work on apatite structures.

References

[1] D. McConnell, Apatite, Its Crystal Chemistry, Mineralogy Utilization and Geologic and Biologic Occurrences, *Applied Mineralogy* Vol. 5, Springer-Verlag, Wien (1973).
[2] A. Vassilikou-Dova, I.M. Kalogeras, B. Macalik and C.A. Londos, *J. Appl. Phys.* **85** (1999) 352.
[3] E.O. Rausch, Thesis, Georgia Institute of Technology (1976).
[4] R.A. Young, R.A.W. van der Lugt and J.C. Elliot, *Nature* **223** (1969) 729.
[5] E.J. Young, A.T. Myers, E.L. Munson and N.M. Conklin, *U.S. Geol. Survey Prof. Paper 650*, **D84** (1969).
[6] P.P. Phakey and J.R. Leonard, *J. Appl. Cryst.* **3** (1970) 38.